



## Removal of roxarsone from synthetic livestock wastewater by sodium alginate loading with micro-scale zerovalent iron

Yue Yin<sup>a</sup>, Jing Zhang<sup>b</sup>, Junfeng Wan<sup>a,c,\*</sup>, Jian Gao<sup>a</sup>, Yan Wang<sup>a</sup>

<sup>a</sup>School of Chemical Engineering and Energy, Zhengzhou University, 100 Science Avenue, China, Tel. +86 371 67 78 10 62; Fax: +86 371 67 78 18 01; email: wanjunfeng@zzu.edu.cn (J. Wan)

<sup>b</sup>Institute of Environmental Planning and Management, College of Environmental Science and Engineering, Tongji University, Siping Rd. 1239, Shanghai 200092, China

<sup>c</sup>Henan Center for Outstanding Overseas Scientists, Zhengzhou, China

Received 2 March 2018; Accepted 5 December 2018

### ABSTRACT

Roxarsone (ROX) as a feed additive in livestock industry could be transported and migrated with manure in soil and aquatic environments, which pose a serious environmental problem due to the long-term accumulation and exposure of arsenic (As). In this study, sodium alginate (SA) loaded micro-scale zerovalent iron (ZVI) was chosen as one macromolecular polymer adsorbent in order to remove residual ROX from synthetic livestock wastewater. The results showed that the maximum adsorption capacity of SA-ZVI for ROX were about 156.4 mg ROX g<sup>-1</sup>. The possible adsorptive mechanism is mainly due to the reaction of hydrogen bonding and electrostatic interactions. Furthermore, the results documented that about 93% of total As sequestered by SA-ZVI could be recovered and the content of As in the recovered product was 105.64 ± 1.58 mg As g<sup>-1</sup>.

*Keywords:* Roxarsone; Livestock wastewater; SA-ZVI; As removal and recovery

### 1. Introduction

Roxarsone (ROX) (3-nitro-4-hydroxyphenylarsonic acid) as one of arsenic (As)-containing feed additives is widely used in livestock and poultry breeding to improve feed efficiency and promote animal growth [1,2]. Up to now, ROX was fed to about 88% of the 9 billion broiler chickens each year in USA. It reported that more than 90% of ROX in feeding was released with manure to environment after the animal digestion [3,4]. During the livestock wastewater treatment process, ROX as a typical organoarsenic compound could be biologically degraded into inorganic As (i.e., As<sup>III</sup> and As<sup>V</sup>) [1]. Hence, a large amount of residual ROX could be discharged and accumulated in the wastewater treatment process and thus would lead to a high ecological risk in the aquatic environment [5]. Additionally, the long-term exposure of ROX and its metabolic products

would influence the biological removal of chemical oxygen demand, nitrogen, and phosphorus [6–8].

Adsorption as one of efficient techniques could be utilized to remove heavy metals from wastewater [9]. Previous studies reported that natural adsorbents such as activated carbons, zeolite, and metal oxides could be used to adsorb ROX [10,11]. However, the corresponding adsorptive capacity of abovementioned adsorbents is limited. Recently, many natural adsorbents were modified in order to increase the adsorptive capacity via loading polymers such as chitosan-based copolymers and modified multi-walled carbon nanotubes [12,13]. Sodium alginate (SA) is a kind of natural hydrophilic organic macromolecule polymer which has a high activity with carbonyl and hydrogen groups. In fact, SA is used as an efficient adsorbent to remove heavy metal ions from wastewater treatment in many fields [14]. However, the organic polymers

\* Corresponding author.

such as alginate have a relatively poor mechanical strength in aqueous solution, which limited its application for the removal of heavy metals in the real engineering. As a result, the modification of the polymers is recently carried out in order to enhance their adsorption capacity and the stability [15]. Nowadays, zerovalent iron (ZVI) is used widely as an effective reactant to remove many pollutants such as heavy metals (e.g., As) and chlorinated organic compounds from polluted groundwater [16]. However, the agglomeration, deactivation, and high mobility in the aqueous solution are the major challenges for single use of nano and micro-scale ZVI in environmental remediation. Besides, how to recovery the pollutants (As, Cu, etc.) adsorbed by ZVI should be considered [17]. In order to resolve abovementioned problems, the research on the preparation and application of novel composite adsorbent is becoming a hot issue in the remediation of metal-polluted environment [18].

In this study, the micro-scale ZVI loaded on SA was prepared as a novel composite adsorbent in order to remove ROX from livestock wastewater. The main factors including reaction time, pH, and initial concentration of ROX on the adsorption were also investigated. Furthermore, the adsorbed SA-ZVI was treated by a series of thermal and chemical processes in order to recover As.

## 2. Materials and methods

### 2.1. Chemicals

The physicochemical properties of ROX (purity: 98%, Rongyao Biotech. Co., Ltd., China) are shown in Table 1. All other chemicals are of analytical grade and purchased from Beijing Chemical Reagent Factory, Beijing, China.

### 2.2. Synthesis of SA-ZVI

The 2.0 g SA was added into 100 mL of deionized water until SA dissolved completely. 2.0 g micro-scale ZVI powder ( $\varnothing = 0.15$  mm) was gently added into the SA solution and stirred for 5 min. The mixed SA-ZVI solution was slowly dripped by peristaltic pump into 200 mL solution (3%  $\text{CaCl}_2$  and 10% ethanol) under 30°C. After 1 h of reaction, the SA-ZVI beads were obtained through the filtration and vacuum freeze-drying.

### 2.3. Adsorption experiment

The concentration of ROX was evaluated by simulated solutions instead of the typical livestock wastewater.

The synthetic livestock wastewater was prepared consisting of sodium propionate (1,540),  $\text{NH}_4\text{Cl}$  (300),  $\text{K}_2\text{HPO}_4$  (56),  $\text{KH}_2\text{PO}_4$  (28),  $\text{KHCO}_3$  (100),  $\text{FeSO}_4 \cdot 7\text{H}_2\text{O}$  (50),  $\text{MgSO}_4 \cdot 7\text{H}_2\text{O}$  (100),  $\text{CaCl}_2$  (20),  $\text{CoCl}_2$  (0.2),  $\text{ZnSO}_4 \cdot 7\text{H}_2\text{O}$  (2),  $\text{H}_3\text{BO}_3$  (1),  $\text{MnSO}_4$  (1),  $\text{CuSO}_4 \cdot 5\text{H}_2\text{O}$  (2),  $\text{NiCl}_2 \cdot 6\text{H}_2\text{O}$  (0.4), all expressed in  $\text{mg L}^{-1}$  [19]. The adsorbent dosage was 1.0  $\text{g L}^{-1}$ . Firstly, the adsorption of ROX by SA-ZVI was evaluated at various initial value of pH (3.0, 6.0, 7.0, 8.0, 9.0, 12.0). Secondly, the initial concentrations of ROX were changed at 10, 20, 50, 100, 200, and 500  $\text{mg L}^{-1}$ . The water samples were extracted and analyzed at the time of 1, 5, 10, 30, 60, 120, 200, 300, and 600 min.

### 2.4. As recovery

After adsorption by SA-ZVI, the adsorbed SA-ZVI samples were burned under 600°C in muffle furnace for 4 h. The obtained powder was dissolved with nitric acid solution (1.0  $\text{mol L}^{-1}$ ) and the dissolved supernatant was collected and adjusted pH to 12.0 with the addition of NaOH solution (1.0  $\text{mol L}^{-1}$ ). The supernatant and precipitate were separated by centrifugation at 4,500 rpm for 15 min. The excess amount of  $\text{Ca}(\text{NO}_3)_2$  (the molar ratio of added Ca to the adsorbed As was controlled between 1.5 and 2.0) was added into the supernatant and the pH of the supernatant was adjusted to 7.5 with addition of nitric acid solution (0.1  $\text{mol L}^{-1}$ ). After 15 min of reaction, the formed precipitates were centrifuged at 8,000 rpm and dried at 105°C.

### 2.5. Analytical methods

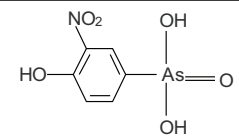
The content of total As was determined by hydride generation atomic fluorescence spectrometry. ROX was determined by the high-performance liquid chromatography with UV detector at 266 nm. The scanning electron microscopy (SEM) images were obtained at 15.0 kV on a cold field SEM after gold plating. Infrared spectra (4,000–400  $\text{cm}^{-1}$ ) were recorded on an FT-IR spectrometer. The crystal morphology was determined by X-ray diffraction spectrum (XRD).

## 3. Results and discussion

### 3.1. Characterization of adsorbents

As shown in Fig. 1(a), SA-ZVI had a rough surface and a loose internal structure. The EDX analysis (Fig. 1(c)) proved that the content of iron on the surface of the particle reached 18.08%. Moreover, XRD analysis (Fig. 1(b)) documented that a diffraction peak at  $2\theta = 44^\circ$  appeared for SA-ZVI, which is

Table 1  
Physicochemical properties of ROX

Name	Chemical formula	Molecular weight ( $\text{g mol}^{-1}$ )	pKa	Melting point ( $^\circ\text{C}$ )	Solubility ( $\text{g L}^{-1}$ )	Molecular structure
ROX	$\text{C}_6\text{H}_6\text{AsNO}_6$	263.04	4.49/5.74/9.13	$\geq 300$	1.0	

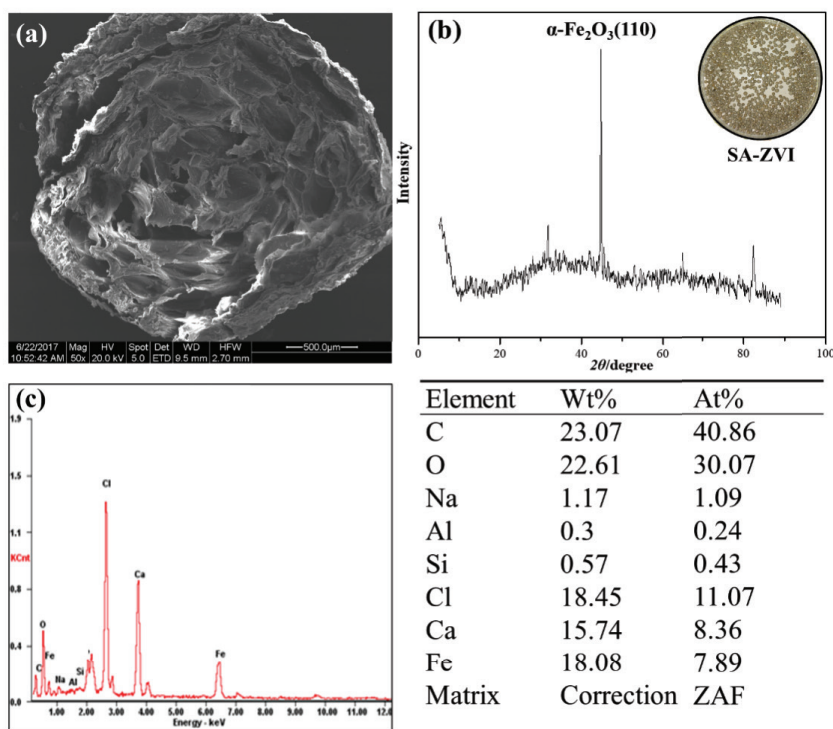


Fig. 1. The characteristic of SA-ZVI before adsorption: the analysis by (a) SEM, (b) XRD, and (c) EDX.

consistent with the characteristic peaks of the  $\alpha\text{-Fe}_2\text{O}_3$  (110) of the body-centered cubic structure [20]. The abovementioned results demonstrated that the part of ZVI was oxidized and some iron oxides crystals were formed during the preparation of SA-ZVI.

### 3.2. Effect of initial pH

The pH of real livestock wastewater is usually ranged from 6.0 to 9.0 [21–23]. Hence, the initial pH of this experiment was ranged from 3.0 to 12.0. The effect of the initial pH value on the ROX adsorption by SA-ZVI was studied as shown in Fig. 2, where  $q_e$  is the maximum amount of ROX adsorbed by SA-ZVI ( $\text{mg g}^{-1}$ ) at equilibrium time. The equilibrium maximum uptake of ROX ( $q_e$ ) was arrived when the initial pH was 6.0. With the increase of the initial pH, the maximum adsorption capacity of ROX was dropped obviously. When  $\text{pH} < 6$ , it is expected that there could be some release of Fe, so it could influence the combination of As and Fe to reduce the adsorption efficiency. Therefore, the pH of the livestock wastewater should be controlled between 6.0 and 7.0 in order to adequately adsorb ROX by SA-ZVI. On the other hand, the results showed that the adsorption mechanism was closely related with the pH.

### 3.3. Adsorption kinetics

Kinetic tests were performed at different concentrations of ROX at  $\text{pH} = 6.0$  under 298 K. As shown in Fig. 3, the adsorption rate of ROX was fast during the first 120 min, and the dynamic equilibrium of the adsorption reached after 300 min of reaction. At the beginning of the adsorption, a

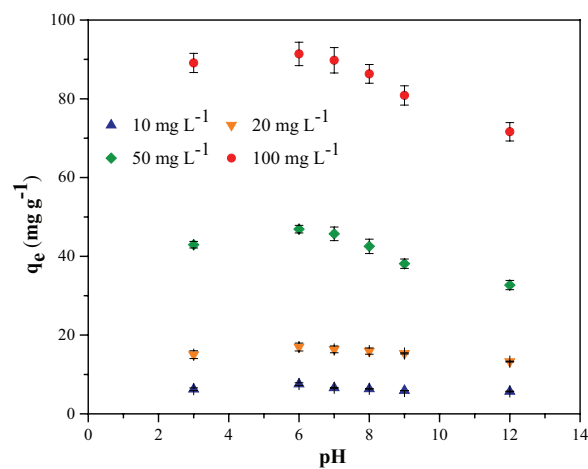


Fig. 2. Effect of the initial pH value on the adsorption of ROX by SA-ZVI.

rapid adsorption process occurred on the surface of SA-ZVI. The pseudo-first-order and pseudo-second-order kinetic models were applied for the adsorption of SA-ZVI. The results showed that the adsorption process is better fitted with the pseudo-second order model ( $R^2 = 0.99$ ), compared with the pseudo-first-order model ( $R^2 = 0.97$ ). Hence, the chemical adsorption probably occurred during the process of the adsorption of ROX by SA-ZVI [24].

### 3.4. Isotherm adsorption

Four isotherm adsorption models were utilized to simulate the isotherm adsorption of ROX by SA-ZVI in

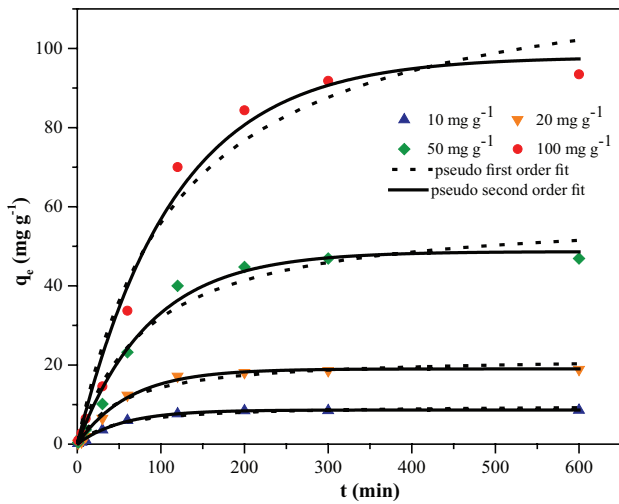


Fig. 3. Kinetics of ROX adsorption by SA-ZVI.

this work, and isothermal parameters were shown in Table 2. Firstly, the Langmuir isotherm is given as Eq. (1). The Langmuir isotherm model is based on an ideal adsorption process that is homogeneous monolayer adsorption, and the energy of each adsorption site remains unchanged [25].

$$q_e = \frac{q_m K_L c_e}{1 + K_L c_e} \quad (1)$$

where  $q_m$  is the maximum adsorption capacity,  $K_L$  is the Langmuir constant,  $c_e$  is equilibrium concentration of ROX in the solution ( $\text{mg L}^{-1}$ ), and  $q_e$  is the amount of ROX adsorbed by adsorbents ( $\text{mg g}^{-1}$ ) at equilibrium time.

Freundlich isotherm model is usually applicable to the adsorption process of heterogeneous surfaces [26]. As an empirical model, Freundlich isotherm could be given as Eq. (2).

$$q_e = K_F c_e^{1/n} \quad (2)$$

where  $K_F$  and  $n$  are the Freundlich constants related to the adsorption capacity and adsorption intensity of the sorbent, respectively. It is generally believed that adsorption becomes easy when  $1/n = 0.1\text{--}0.5$ , while adsorption is difficult to be occurred if  $1/n > 2$ .

Koble–Corrigan (K–C) model is three-parameter equation for the representing equilibrium adsorption data [27]. It is a combination of the Langmuir and Freundlich isotherm type models and is given as Eq. (3).

$$q_e = \frac{A c_e^n}{1 + B c_e^n} \quad (3)$$

where  $A$ ,  $B$ , and  $n$  are the K–C parameters.

The derivation of the Temkin isotherm assumes that the fall in the heat of adsorption is linear rather than logarithmic [28]. The Temkin isotherm is given as Eq. (4).

Table 2  
Isothermal parameters for ROX adsorption on SA-ZVI

Langmuir model		Freundlich model	
$K_L$	0.07768	$K_F$	26.16752
$q_m$ ( $\text{mg g}^{-1}$ )	156.41	$1/n$	0.3166
$R^2$	0.94	$R^2$	0.80
Koble–Corrigan model		Temkin model	
$A$	6.57279	$A$	-3.27394
$B$	0.04555	$B$	28.78818
$n$	1.41352	$R^2$	0.93
$R^2$	0.95		

$$q_e = A + B \ln c_e \quad (4)$$

where  $A$  and  $B$  are the Temkin parameters, and  $c_e$  is equilibrium concentration of ROX in the solution ( $\text{mg L}^{-1}$ ).

The isothermal adsorption process of SA-ZVI to ROX was studied at  $\text{pH} = 6.0$  under 298 K. The experimental data were fitted by the four isothermal adsorption models as shown in Fig. 4. Based on the values of  $R^2$ , the best isothermal adsorption model was K–C ( $R^2 = 0.95$ ), which was followed by Langmuir ( $R^2 = 0.94$ ), Temkin ( $R^2 = 0.93$ ), and Freundlich ( $R^2 = 0.80$ ) models. Additionally, the maximum adsorption capacity to ROX calculated through the Langmuir model was  $156.4 \text{ mg g}^{-1}$ . Besides, the parameter  $1/n$  obtained from Freundlich isothermal are between 0.32 and 0.33 ( $< 0.5$ ) which revealed that the adsorption process may be occurred easily [29].

## 4. Discussion

### 4.1. Adsorption mechanism of ROX

Normally, the mechanisms of adsorption are complex including electrostatic, hydrogen bonding, acid–base interactions, etc. [30]. The results documented that the adsorption capacity of ROX by SA-ZVI can be influenced effectively by the pH value. The optimal range of the pH value is between 6.0 and 7.0. In fact, the acidity values ( $\text{p}K_a$ ) of ROX ( $\text{p}K_{a1} = 3.49$ ,  $\text{p}K_{a2} = 5.74$ ,  $\text{p}K_{a3} = 9.13$ ) determine the existence form of ROX under various pH (Fig. 5(a)) [31]. The corresponding ROX exists in  $\text{HAsO}_3\text{R}^{2-}$  (where R is the aromatic group) at  $\text{pH} = 6.0$  [10]. On the other hand, the adsorbent surface charge is decided by the electric charge presented at interface and on dispersion into polar media such as water, while the charge on adsorbents could also be modified by grafting of particular species onto the materials by protonation or deprotonation. Accordingly, SA-ZVI containing a large amount of  $-\text{COO}^-$  exhibited polyanionic behavior in aqueous solution. Under acidic conditions, the  $-\text{COO}^-$  could be converted into  $-\text{COOH}$ , and the surface existed a large amount of positive charge. Hence, SA-ZVI adsorbed  $\text{H}_2\text{AsO}_3\text{R}^-$  and  $\text{HAsO}_3\text{R}^{2-}$  mainly by electrostatic interactions. Furthermore, under alkaline conditions, the adsorption capacity of ROX decreased because the surface charge of SA-ZVI was changed. Besides, the interaction of Fe–O–As bonds was probably the main mechanism instead of electrostatic interaction for the ROX removal, which was demonstrated by FT-IR analysis.

In Fig. 5(b), these samples were analyzed by FT-IR before and after adsorption. After adsorption of SA-ZVI, the characteristic absorption peaks of benzene vibration were detected at 1,605 and 1,448  $\text{cm}^{-1}$ , which indicated that ROX was adsorbed on the surface. Meanwhile, the free hydroxyl was detected at 3,496 and 3,512  $\text{cm}^{-1}$  before adsorption, while the intermolecular hydrogen bonds were detected at 3,268 and 3,273  $\text{cm}^{-1}$  after adsorption [32,33]. The results indicated that intermolecular hydrogen bonds may be involved in the adsorption process of ROX [34]. In addition, the introduction of ZVI into SA not only increased the mechanical strength of the adsorbent, but also increased the adsorption of As due to the high affinity of iron to As [35,36]. It was reported that ZVI could reduce the mobility of As by the formation of amorphous  $\text{FeAsO}_4 \cdot \text{H}_2\text{O}$  or soluble secondary oxidation minerals such as  $\text{FeAsO}_4 \cdot 2\text{H}_2\text{O}$  [37]. Bonds such as  $\text{FeOOH-As}$  and  $\text{As-O-Fe}$  were contributed to the adsorption of arsenic by iron [10]. In many cases, iron oxides and their hydrated compounds could form stable coordination bonds with As. Moreover, it also demonstrated that  $\text{Fe-OH}_2$  may interact with ROX anion species. The positively charged surface

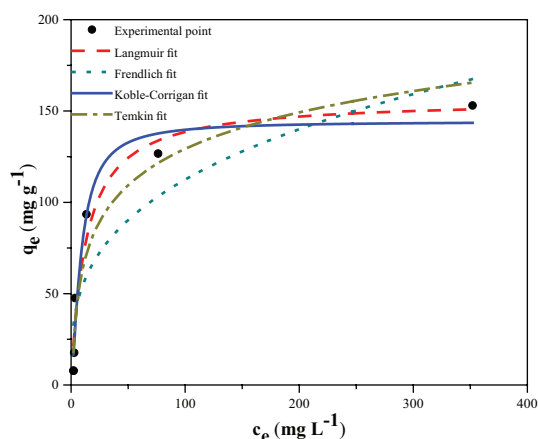


Fig. 4. Isothermal adsorption of ROX by SA-ZVI under 298 K.

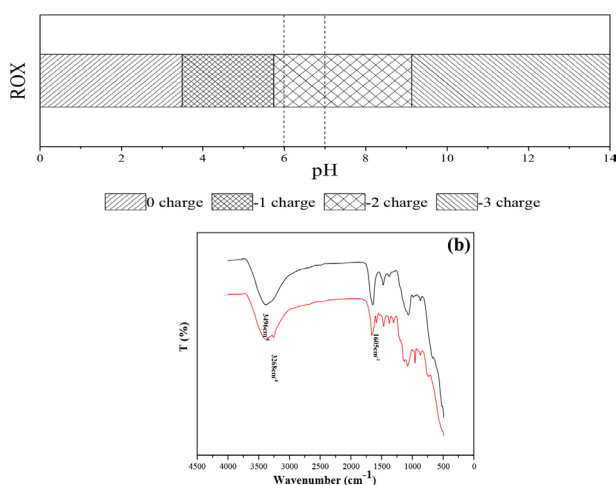


Fig. 5. ROX forms at various (a) pH; (b) FT-IR of SA-ZVI before (black) and after adsorption (red).

$\text{Fe-OH}_2$  groups can bind with ROX via the O- and N-heteroatom sites of ROX as complexes ( $\text{Fe-O-As}$  and  $\text{Fe-O-N}$ ) [38].

Some reported adsorbents were modified in order to remove ROX as shown in Table 3. The maximum removal capacity ( $q_m$ ) of SA-ZVI ( $156.4 \text{ mg g}^{-1}$ ) was much higher than the modified multi-walled carbon nanotubes and goethite nanoparticles. Compared with Materials Institute Lavoisier-100-Fe and chitosan-based copolymers SA-ZVI was cheap and easy to synthesize. Regarding the mechanisms of ROX removal, it should be noted that ROX could be interacted with various functional groups (e.g., hydrogen bonding) presented in different materials.

#### 4.2. Evaluation of recovered product

The As recovery experiment was carried out through a series of physicochemical process. The total As content of recovered solid mixture was  $105.64 \pm 1.58 \text{ mg As g}^{-1}$ , which means that 92.8% of adsorbed arsenic was recovered. It can be seen from Fig. 6 that the characteristic peaks of XRD of

Table 3  
Adsorption capacity of ROX onto various adsorbents

Adsorbents	$q_m$ ( $\text{mg g}^{-1}$ )	Dominant mechanisms	References
Iron modified multi-walled carbon nanotubes	25.8	Electrostatic interactions	[39]
Goethite nanoparticles	19.2	Electrostatic interactions	[38]
Ammonium persulfate- $\text{SiO}_2$	157.0	Acid-base interactions	[40]
Molecularly imprinted polymers	100.0	Acid-base interactions	[40]
Materials Institute Lavoisier-100-Fe	387	Hydrogen bonding	[41]
Chitosan-based copolymers	473	Hydrogen bonding	[42]
SA-ZVI	156.4	Hydrogen bonding	This study

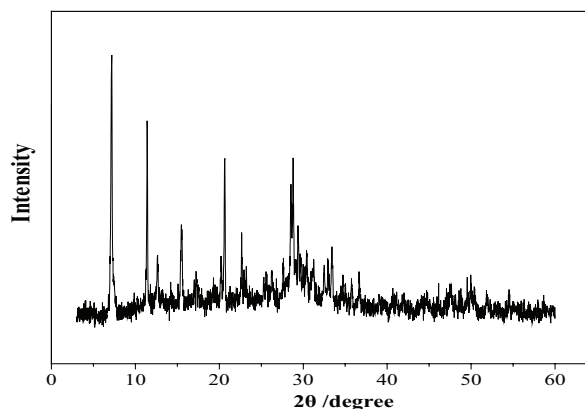


Fig. 6. XRD patterns of final recovered products.

the solid mixture have the high similarity to the characteristic peaks of  $\text{CaAs}_2\text{O}_7$ ,  $\text{CaAs}_3(\text{OH})\cdot 2\text{H}_2\text{O}$ , and  $\text{Ca}_3(\text{AsO}_4)_2\cdot 8\text{H}_2\text{O}$ , revealed that the main component of the products could be possible a mixture of these three calcium and arsenic compounds [43].

## 5. Conclusions

The equilibrium adsorption of ROX onto SA-ZVI was simulated by the four isotherms models (Langmuir, Freundlich, K–C, and Temkin models), in which the K–C equation was the best ideal model to fit the equilibrium data. The dynamic adsorption process could be predicted by pseudo-second-order model. The adsorption of ROX by SA-ZVI was significantly affected by the pH value. The optimum range of pH was between 6.0 and 7.0. The results documented that SA-ZVI could not only efficiently remove ROX from synthetic livestock wastewater, but also recovery over 90% of As.

## Acknowledgment

The authors thank the National Natural Science Foundation of China (No. 21107100), Henan Provincial Science and Technology Development Program (No. 172102410031), and Program of Processing and Efficient Utilization of Biomass Resources of Henan Center for Outstanding Overseas Scientists (GZS2018004) for the financial support of this study.

## References

- [1] J.R. Garbarino, A.J. Bednar, D.W. Rutherford, R.S. Beyer, R.L. Wershaw, Environmental fate of roxarsone in poultry litter. I. Degradation of roxarsone during composting, *Environ. Sci. Technol.*, 37 (2003) 1509.
- [2] K.C. Makris, J. Salazar, S. Quazi, S.S. Andra, D. Sarkar, S.B. Bach, R. Datta, Controlling the fate of roxarsone and inorganic arsenic in poultry litter, *J. Environ. Qual.*, 37 (2008) 963.
- [3] J.H. Walrod, D. Burriss, L.Y. Blue, G.E. Beck, D.A. Atwood, Arsenic mobility in Karnak soils after multi-year application of poultry litter containing roxarsone, *Main Group Chem.*, 15 (2016) 365–373.
- [4] Q.L. Fu, J.Z. He, H. Gong, L. Blaney, D.M. Zhou, Extraction and speciation analysis of roxarsone and its metabolites from soils with different physicochemical properties, *J. Soils Sediments*, 16 (2016) 1–12.
- [5] B.K. Mandal, K.T. Suzuki, Arsenic round the world: a review, *Talanta*, 58 (2002) 201–235.
- [6] W. Zhang, F. Xu, J. Han, Q. Sun, K. Yang, Comparative cytotoxicity and accumulation of Roxarsone and its photodegradates in freshwater Protozoan *Tetrahymena thermophila*, *J. Hazard. Mater.*, 286 (2015) 171–178.
- [7] K.E. Nachman, P.A. Baron, R. Georg, K.A. Francesconi, N.A. Ana, D.C. Love, Roxarsone, inorganic arsenic, and other arsenic species in chicken: a U.S.-based market basket sample, *Environ. Health Perspect.*, 121 (2013) 818–824.
- [8] H. Liu, G. Wang, J. Ge, L. Li, G. Chen, Fate of roxarsone during biological nitrogen removal process in wastewater treatment systems, *Chem. Eng. J.*, 255 (2014) 500–505.
- [9] J. Wan, J. Pressigout, S. Simon, V. Deluchat, Distribution of As trapping along a ZVI/sand bed reactor, *Chem. Eng. J.*, 246 (2014) 322–327.
- [10] W.R. Chen, C.H. Huang, Surface adsorption of organoarsenic roxarsone and arsenic acid on iron and aluminum oxides, *J. Hazard. Mater.*, 227–228 (2012) 378–385.
- [11] Z. Hu, J. Hu, Z. Tong, G. Chen, Adsorption of Roxarsone from Aqueous Solution by Multi-walled Carbon Nanotubes: Equilibrium and Kinetics Studies, International Conference on Environmental Simulation and Pollution Control, 2011, pp. 355–361.
- [12] Y. Yin, Y. Chi, S. Li, J. Wan, Y. Wang, Study on adsorption of roxarsone by CS-ZVI in the livestock wastewater, *Guangdong Chem. Ind.*, 356 (2017) 3–4.
- [13] J.H. Chen, H.T. Xing, H.X. Guo, G.P. Li, W. Weng, S.R. Hu, Preparation, characterization and adsorption properties of a novel 3-aminopropyltriethoxysilane functionalized sodium alginate porous membrane adsorbent for Cr(III) ions, *J. Hazard. Mater.*, 248–249 (2013) 285.
- [14] G. Xie, X. Shang, R. Liu, J. Hu, S. Liao, Synthesis and characterization of a novel amino modified starch and its adsorption properties for Cd(II) ions from aqueous solution, *Carbohydr. Polym.*, 84 (2011) 430–438.
- [15] F. Fu, D.D. Dionysiou, H. Liu, The use of zero-valent iron for groundwater remediation and wastewater treatment: a review, *J. Hazard. Mater.*, 267 (2014) 194–205.
- [16] S. Song, A. Lopezvaldivieso, D.J. Hernandezcampos, C. Peng, M.G. Monroyfernandez, I. Razosoto, Arsenic removal from high-arsenic water by enhanced coagulation with ferric ions and coarse calcite, *Water Res.*, 40 (2006) 364.
- [17] T. Liu, L. Zhao, D. Sun, X. Tan, Entrapment of nanoscale zero-valent iron in chitosan beads for hexavalent chromium removal from wastewater, *J. Hazard. Mater.*, 184 (2010) 724–730.
- [18] C.Y. Li, S.B. Wu, F. Sun, T. Lv, R.J. Dong, C.L. Pang, Performance of lab-scale tidal flow constructed wetlands treating livestock wastewater, *Adv. Mater. Res.*, 518–523 (2012) 2631–2639.
- [19] L. Liu, H.Z. Kou, W. Mo, H. Liu, Y. Wang, Surfactant-assisted synthesis of alpha- $\text{Fe}_2\text{O}_3$  nanotubes and nanorods with shape-dependent magnetic properties, *J. Phys. Chem. B*, 110 (2006) 15218–15223.
- [20] H. Lee, M. Shoda, Removal of COD and color from livestock wastewater by the Fenton method, *J. Hazard. Mater.*, 153 (2008) 1314–1319.
- [21] H. Liansheng, L. Hongliang, X. Beidou, Z. Yingbo, Effects of effluent recirculation in vertical-flow constructed wetland on treatment efficiency of livestock wastewater, *Water. Sci. Technol.*, 54 (2006) 137.
- [22] B.Y. Tak, B.S. Tak, Y.J. Kim, Y.J. Park, Y.H. Yoon, G.H. Min, Optimization of color and COD removal from livestock wastewater by electrocoagulation process: application of Box–Behnken design (BBD), *J. Ind. Eng. Chem.*, 28 (2015) 307–315.
- [23] R.P. Han, J.J. Zhang, P. Han, Y.F. Wang, Z.H. Zhao, M.S. Tang, Study of equilibrium, kinetic and thermodynamic parameters about methylene blue adsorption onto natural zeolite, *Chem. Eng. J.*, 145 (2009) 496–504.
- [24] I. Langmuir, The constitution and fundamental properties of solids and liquids, *J. Franklin Inst.*, 184 (1916) 102–105.
- [25] H. Freundlich, Über die adsorption in Lösungen, *Z. Phys. Chem.*, 57u (2017) 384–470.
- [26] R.A. Koble, T.E. Corrigan, Adsorption isotherms for pure hydrocarbons, *Boletín De Pediatría*, 174 (1952) 10–27.
- [27] C. Aharoni, M. Ungarish, Kinetics of activated chemisorption. Part 2. Theoretical models, *J. Chem. Soc., Faraday Trans.*, 73 (1977) 456–464.
- [28] I. Abe, K. Hayashi, T. Hirashima, M. Kitagawa, Relationship between the Freundlich adsorption constants K and 1/N hydrophobic adsorption, *Chemischer Informationsdienst*, 14 (1983) 6450–6453.
- [29] J. Hu, Z. Tong, G. Chen, X. Zhan, Z. Hu, Adsorption of roxarsone by iron (hydr)oxide-modified multiwalled carbon nanotubes from aqueous solution and its mechanisms, *Int. J. Environ. Sci. Technol.*, 11 (2013) 785–794.
- [30] J. Hu, Z. Tong, Z. Hu, G. Chen, T. Chen, Adsorption of roxarsone from aqueous solution by multi-walled carbon nanotubes, *J. Colloid Interface Sci.*, 377 (2012) 355–361.
- [31] W.R. Chen, C.H. Huang, Surface adsorption of organoarsenic roxarsone and arsenic acid on iron and aluminum oxides, *J. Hazard. Mater.*, 227–228 (2012) 378–385.
- [32] B.N. Snegirev, Vibrational spectra of aromatic compounds. XI. Calculation of intensities in the infrared spectrum of toluene, *Opt. Spectrosc.*, 11 (1961) 313–315.

- [33] J. Dong, Yukihiro Ozaki, K. Nakashima, Infrared, Raman, and near-infrared spectroscopic evidence for the coexistence of various hydrogen-bond forms in poly(acrylic acid), *Macromolecules*, 30 (1997) 1111–1117.
- [34] M. Sarker, J.Y. Song, S.H. Jhung, Adsorption of organic arsenic acids from water over functionalized metal-organic frameworks, *J. Hazard. Mater.*, 335 (2017) 162.
- [35] W. Chen, R. Parette, J. Zou, F.S. Cannon, B.A. Dempsey, Arsenic removal by iron-modified activated carbon, *Water. Res.*, 41 (2007) 1851.
- [36] D. Mohan, C.U.P. Jr, Arsenic removal from water/wastewater using adsorbents—a critical review, *J. Hazard. Mater.*, 142 (2007) 1.
- [37] Y. Mamindy-Pajany, C. Hurel, N. Marmier, M. Roméo, Arsenic (V) adsorption from aqueous solution onto goethite, hematite, magnetite and zero-valent iron: effects of pH, concentration and reversibility, *Desalination*, 281 (2011) 93–99.
- [38] D. Kong, L.D. Wilson, Synthesis and characterization of cellulose-goethite composites and their adsorption properties with roxarsone, *Carbohydr. Polym.*, 169 (2017) 282–294.
- [39] L. Poon, S. Younus, L.D. Wilson, Adsorption study of an organo-arsenical with chitosan-based sorbents, *J. Colloid Interface Sci.*, 420 (2014) 136–144.
- [40] W. Fan, X. Zhang, Y. Zhang, P. Wang, L. Zhang, Z. Yin, J. Yao, W. Xiang, Functional organic material for roxarsone and its derivatives recognition via molecular imprinting, *J. Mol. Recognit.*, 31 (2017) 2625–2634.
- [41] Z. Hasan, S.H. Jhung, Removal of hazardous organics from water using metal-organic frameworks (MOFs): plausible mechanisms for selective adsorptions, *J. Hazard. Mater.*, 283 (2015) 329–339.
- [42] O.M. Yaghi, M. O’Keeffe, N.W. Ockwig, H.K. Chae, M. Eddaoudi, J. Kim, Reticular synthesis and the design of new materials, *Nature*, 423 (2003) 705.
- [43] J.V. Bothe, P.W. Brown, CaO-As<sub>2</sub>O<sub>5</sub>-H<sub>2</sub>O System at 23°±1°C, *J. Am. Ceram. Soc.*, 85 (2010) 221–224.